

Zeitschrift für anorganische und allgemeine Chemie

Supporting Information

Mechanism of Dihydrogen Splitting by An Apparent Bimetallic Frustrated Lewis Pair based on Ir(III)/Pt(0)

Juan J. Moreno,* Alejandra Pita-Milleiro, Ana Luque-Gómez, María F. Espada, Joaquín López-Serrano, and Jesús Campos*

Mechanism of Dihydrogen Splitting by An Apparent Bimetallic Frustrated Lewis Pair based on Ir(III)/Pt(0)

Juan J. Moreno,* Alejandra Pita-Milleiro, Ana Luque-Gómez, María F. Espada, Joaquín López-Serrano and Jesús Campos*

Instituto de Investigaciones Químicas (IIQ), Departamento de Química Inorgánica and Centro de Innovación en Química Avanzada (ORFEÓ-CINQA), Universidad de Sevilla and Consejo Superior de Investigaciones Científicas (CSIC), Avenida Américo Vespucio 49, 41092 Sevilla, Spain.

Supporting Information

1. NMR Spectra.....	2
2. Kinetic Isotopic Effect (KIE) Experiments	7
3. X-Ray Characterization.....	8
4. Computational Studies	10
5. References	13

1. NMR Spectra

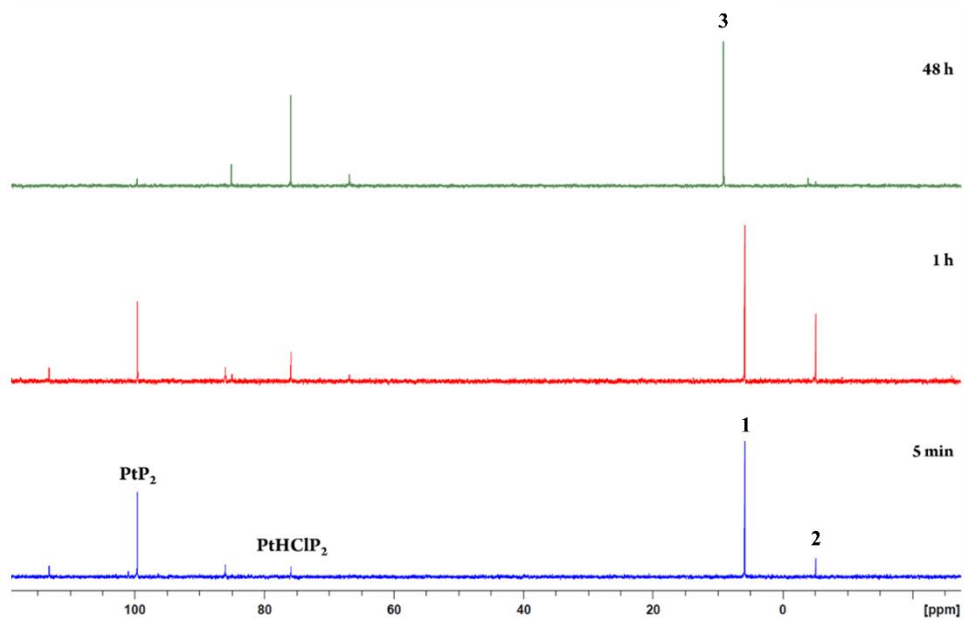


Figure S1. Room temperature evolution of **1** and Pt(PBu₃)₂.

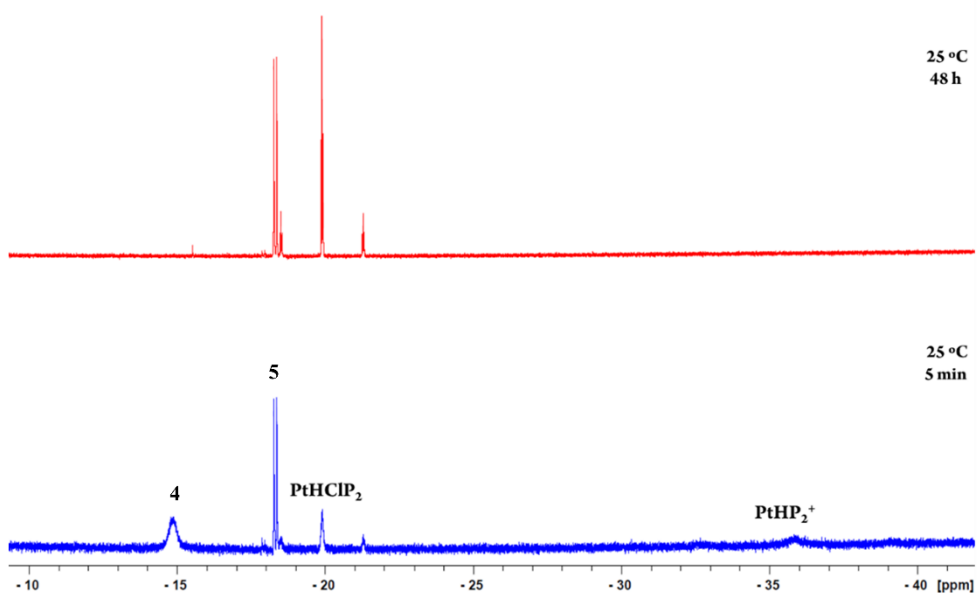


Figure S2. Hydridic region of the ¹H NMR spectrum corresponding to the room temperature heterolytic H₂ splitting by the Ir(III) compound **1** and Pt(PBu₃)₂ after 5 min (bottom) and 48 h (top).

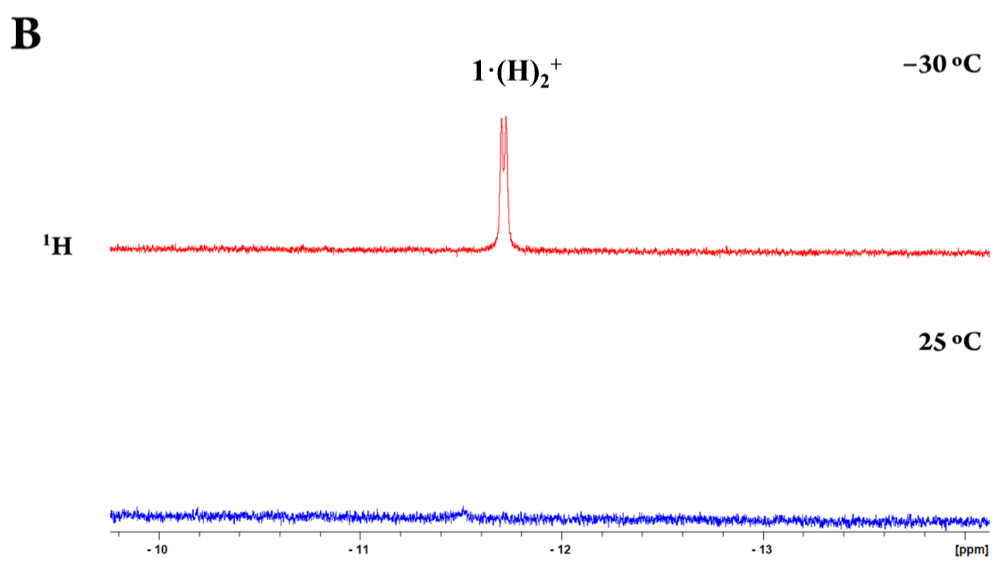
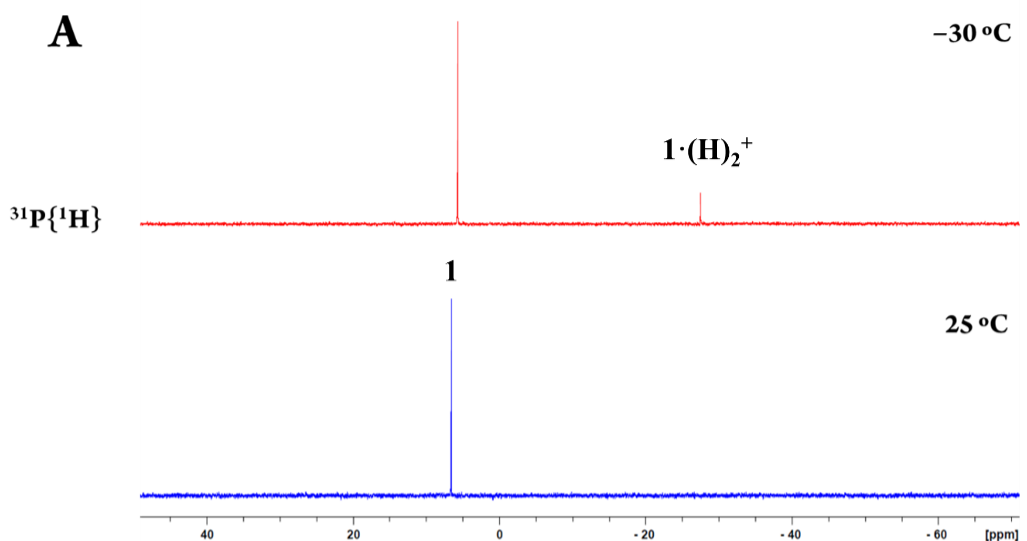


Figure S3. Selected regions of the ${}^{31}\text{P}\{{}^1\text{H}\}$ (A, top) and ${}^1\text{H}$ (B, bottom) NMR spectra of **1** under H_2 atmosphere (1 bar) at $-30\text{ }^{\circ}\text{C}$ and at room temperature.

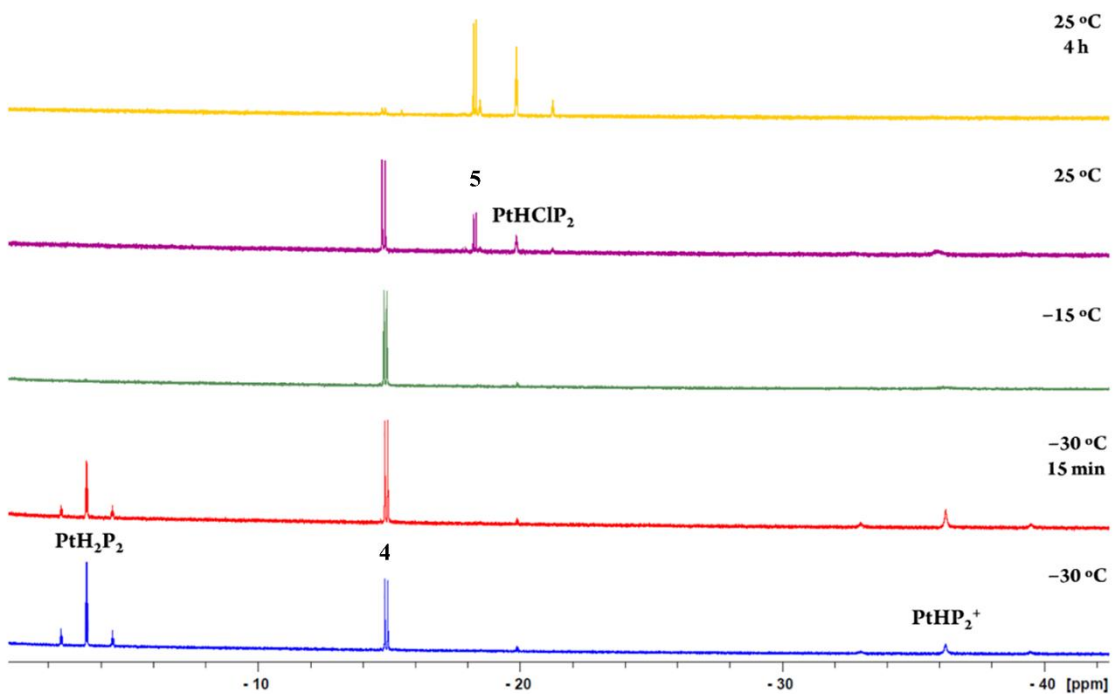


Figure S4. Hydride region (ca. 0 to -40 ppm) of the ^1H NMR spectrum corresponding to the low-temperature NMR monitoring of the reaction between the Ir(III) compound **1**, $\text{Pt}(\text{P}^{\prime}\text{Bu}_3)_2$ and H_2 .

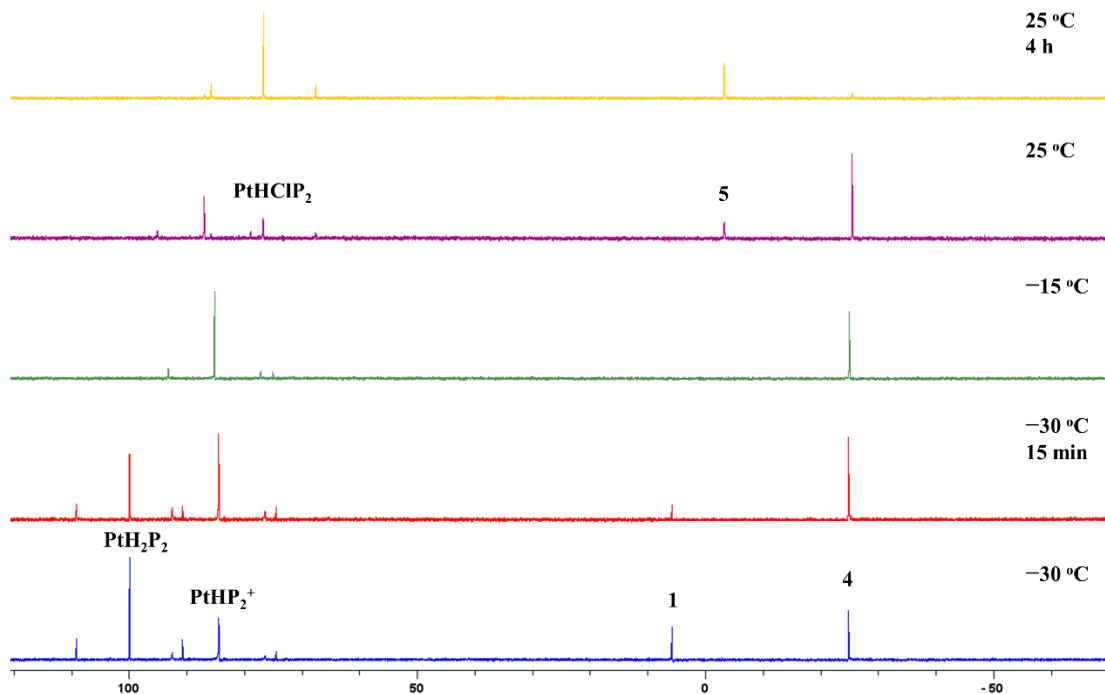


Figure S5. $^{31}\text{P}\{^1\text{H}\}$ NMR spectrum corresponding to the low-temperature NMR monitoring of the reaction between the Ir(III) compound **1**, $\text{Pt}(\text{P}^{\prime}\text{Bu}_3)_2$ and H_2 .

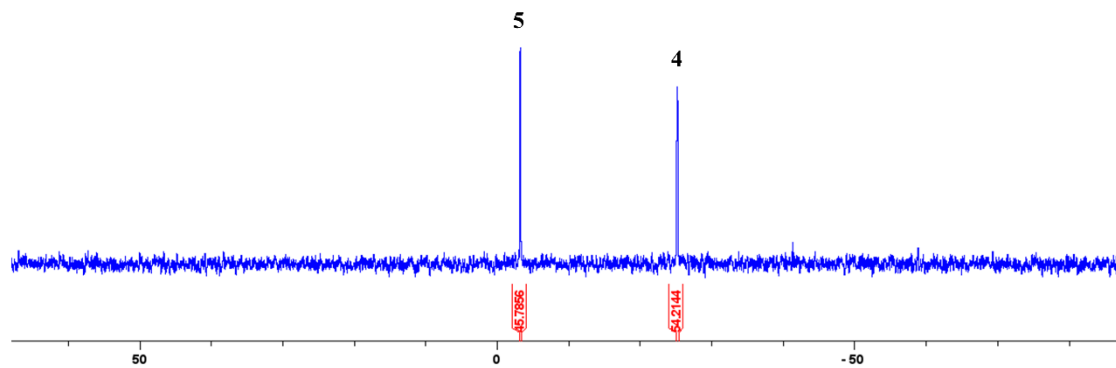


Figure S6. ${}^3\text{P}\{{}^1\text{H}\}$ NMR spectrum of the reaction mixture of *in situ* generated **1:1·(H)₂⁺** solution after addition of one equivalent of NEt_3 .

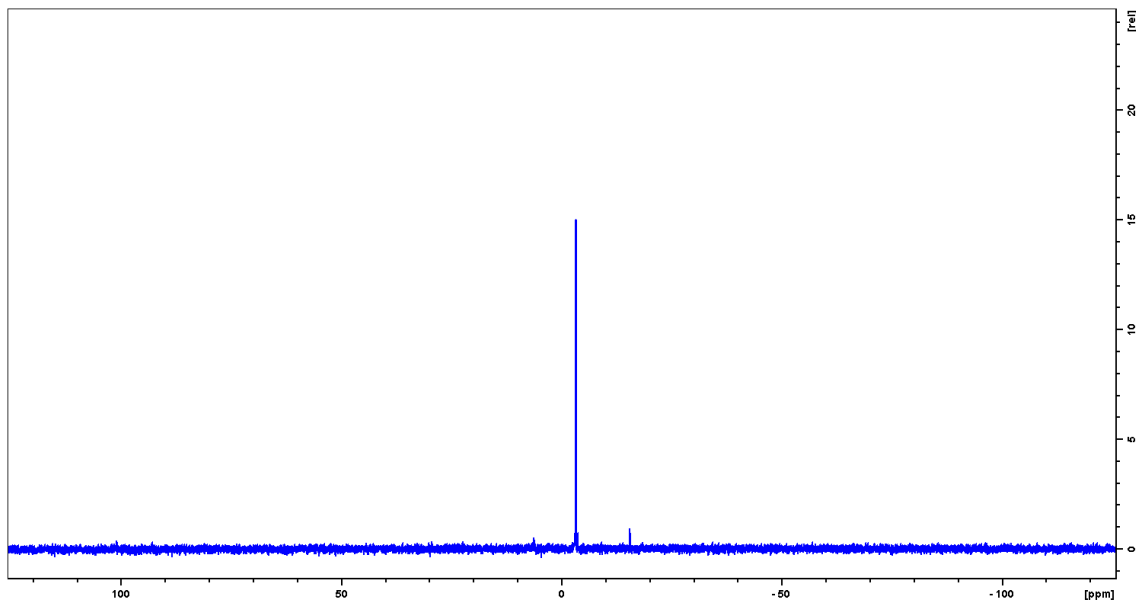


Figure S7. ${}^3\text{P}\{{}^1\text{H}\}$ NMR spectrum of complex **5**.

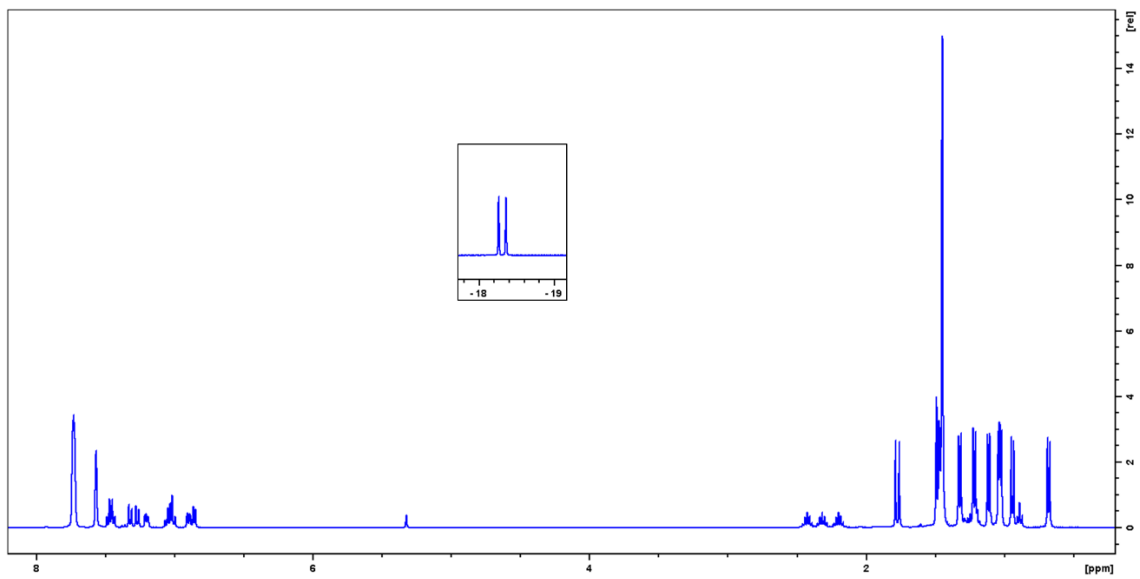


Figure S8. ^1H NMR spectrum of complex 5. Inset shows the hydridic resonance.

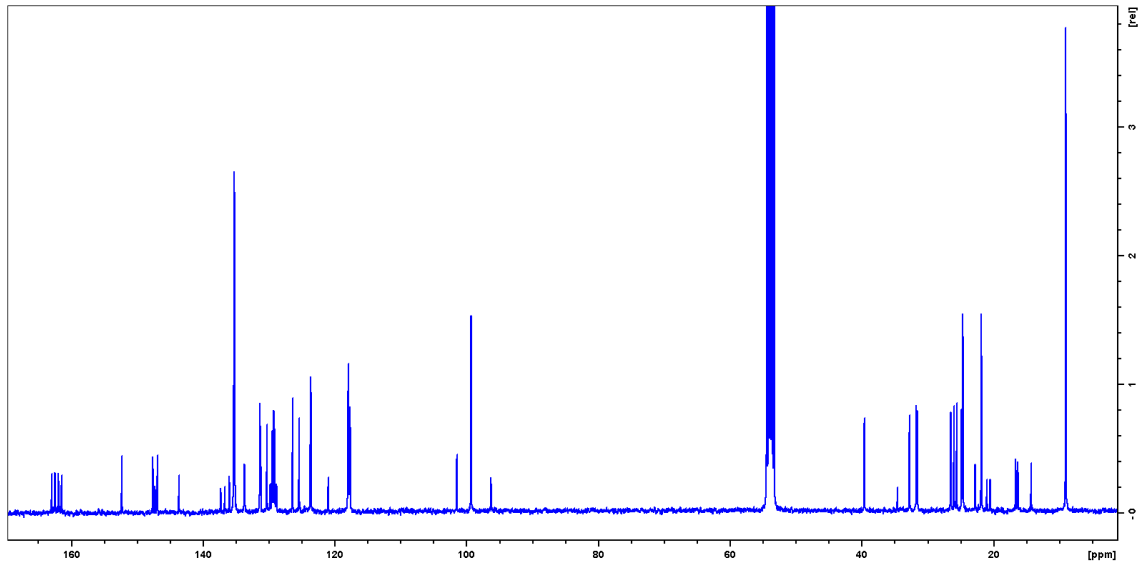


Figure S9. $^{13}\text{C}\{\text{H}\}$ NMR spectrum of complex 5.

2. Kinetic Isotopic Effect (KIE) Experiments

Experiments were performed at $-80\text{ }^{\circ}\text{C}$ in CD_2Cl_2 , and the progress of the reaction was monitored by $^{31}\text{P}\{^1\text{H}\}$ NMR spectroscopy by means of the disappearance of the Pt(0) precursor.

In a representative example, $\text{Pt}(\text{P}'\text{Bu}_3)_2$ (3.1 mg, 0.006 mmol) was placed in a *J. Young* NMR tube and dissolved in CD_2Cl_2 (0.4 mL), the resulting solution was frozen and, then, a solution of compound **1** (10 mg, 0.006 mmol) in CD_2Cl_2 (0.4 mL) was added and then frozen. The inert gas was removed under high vacuum and H_2 or D_2 (1.75 bar) was subsequently added while the solutions remained frozen and unmixed. Finally, the mixture was shaken while kept at $-80\text{ }^{\circ}\text{C}$ and the tube was finally placed into the NMR spectrometer at $-80\text{ }^{\circ}\text{C}$.

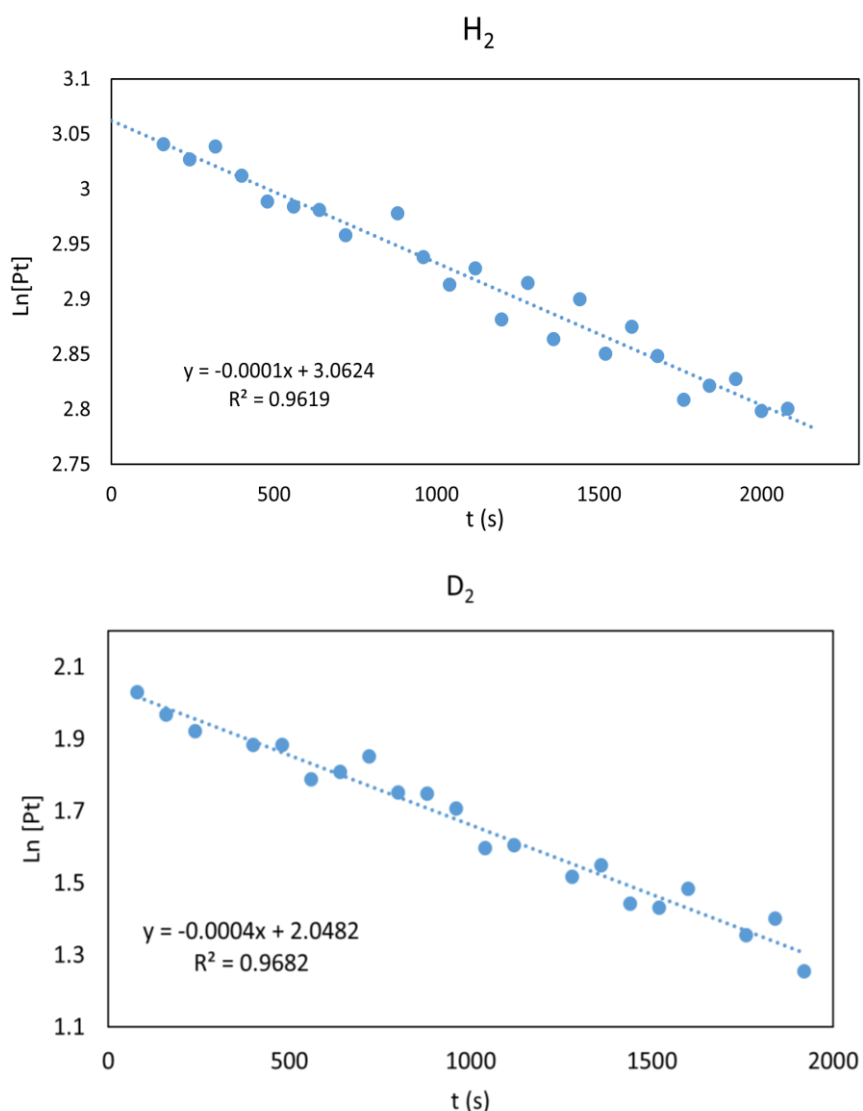


Figure S10. Kinetic profiles for the activation of H_2 and D_2 ($k_{\text{H}}/k_{\text{D}} = 0.33$).

3. X-Ray Characterization

Crystallographic details. Crystals of compound **5** were grown by slow diffusion of hexane into their CH₂Cl₂ solutions. Low-temperature diffraction data were collected on a Bruker APEX-II CCD diffractometer with a Photon III detector and a IμS 3.0 microfocus X-ray source at the Instituto de Investigaciones Químicas, Sevilla. Data were collected by means of ω and φ scans using monochromatic radiation $\lambda(\text{Mo K}\alpha 1) = 0.71073 \text{ \AA}$. The diffraction images collected were processed and scaled using APEX-III software. Using Olex2^[1,2,3], the structure was solved with SHELXS and was refined against F² on all data by full-matrix least squares with SHELXL.^[4] All non-hydrogen atoms were refined anisotropically. Hydrogen atoms were included in the model at geometrically calculated positions and refined using a riding model, except the hydride which has been determined from the Fourier map. The isotropic displacement parameters of all hydrogen atoms were fixed to 1.2 times the U value of the atoms to which they are linked (1.5 times for methyl groups).

A summary of the fundamental crystal and refinement data are given in **Error! No se encuentra el origen de la referencia.** Atomic coordinates, anisotropic displacement parameters and bond lengths and angles can be found in the cif file, which have been deposited in the Cambridge Crystallographic Data Centre with no. 2234614. These data can be obtained free of charge from The Cambridge Crystallographic Data Centre via www.ccdc.cam.ac.uk/data_request/cif.

Table S1. Crystal data and structure refinement for compound **5**.

	5
formula	C ₇₄ H ₇₁ BF ₂₄ IrP
Fw	1650.29
cryst.size, mm	0.35 × 0.28 × 0.18
crystal system	monoclinic
space group	P2 ₁ /c
<i>a</i> , Å	12.8661(4)
<i>b</i> , Å	20.7413(7)
<i>c</i> , Å	27.3249(10)
α , deg	90.00
β , deg	96.600(2)
γ , deg	90.00
<i>V</i> , Å ³	7243.6(4)

<i>T</i> , K	173(2)
<i>Z</i>	4
ρ_{calc} , g cm ⁻³	1.513
μ , mm ⁻¹ (MoK α)	1.969
<i>F</i> (000)	3312.0
absorption corrections	Semi-empirical from equivalents
θ range, deg	4.16 to 50.5
no. of rflns measd	78857
R _{int}	0.0423
no. of rflns unique	13090
no. of params / restraints	980/222
R_1 ($I > 2\sigma(I)$) ^a	0.0363
R_1 (all data)	0.0505
wR_2 ($I > 2\sigma(I)$)	0.0907
wR_2 (all data)	0.0968
Diff.Fourier.peaks min/max, eÅ ⁻³	-1.04/1.59
CCDC number	2234614

4. Computational Studies

Calculations were performed at the DFT level with the Gaussian 09 (Revision D.01) program.^[5] The hybrid functional PBE0^[6] was used throughout the computational study. Geometry optimizations were carried out without geometry constraints, using the 6-31G(d,p)^[7] basis set to represent the C, H, P, and Cl atoms and the Stuttgart/Dresden Effective Core Potential and its associated basis set (SDD)^[8] to describe the Ir, and Pt atoms. Bulk solvent effects (dichloromethane) were included at the optimization stage with the SMD continuum model.^[9] Dispersion effects were accounted for by using Grimme's D3 parameter set with Becke–Johnson (BJ) damping.^[10] The stationary points and their nature as minima or saddle points (TS) were characterized by vibrational analysis, which also produced enthalpy (H), entropy (S) and Gibbs energy (G) data at 298.15 K. The minima connected by a given transition state were determined by perturbing the transition states along the TS coordinate and optimizing to the nearest minimum. 50%-corrected free energy variations (ΔG_{50}), employed to account for translational entropy overestimation,^[11,12] were carried out for direct comparison with related systems.

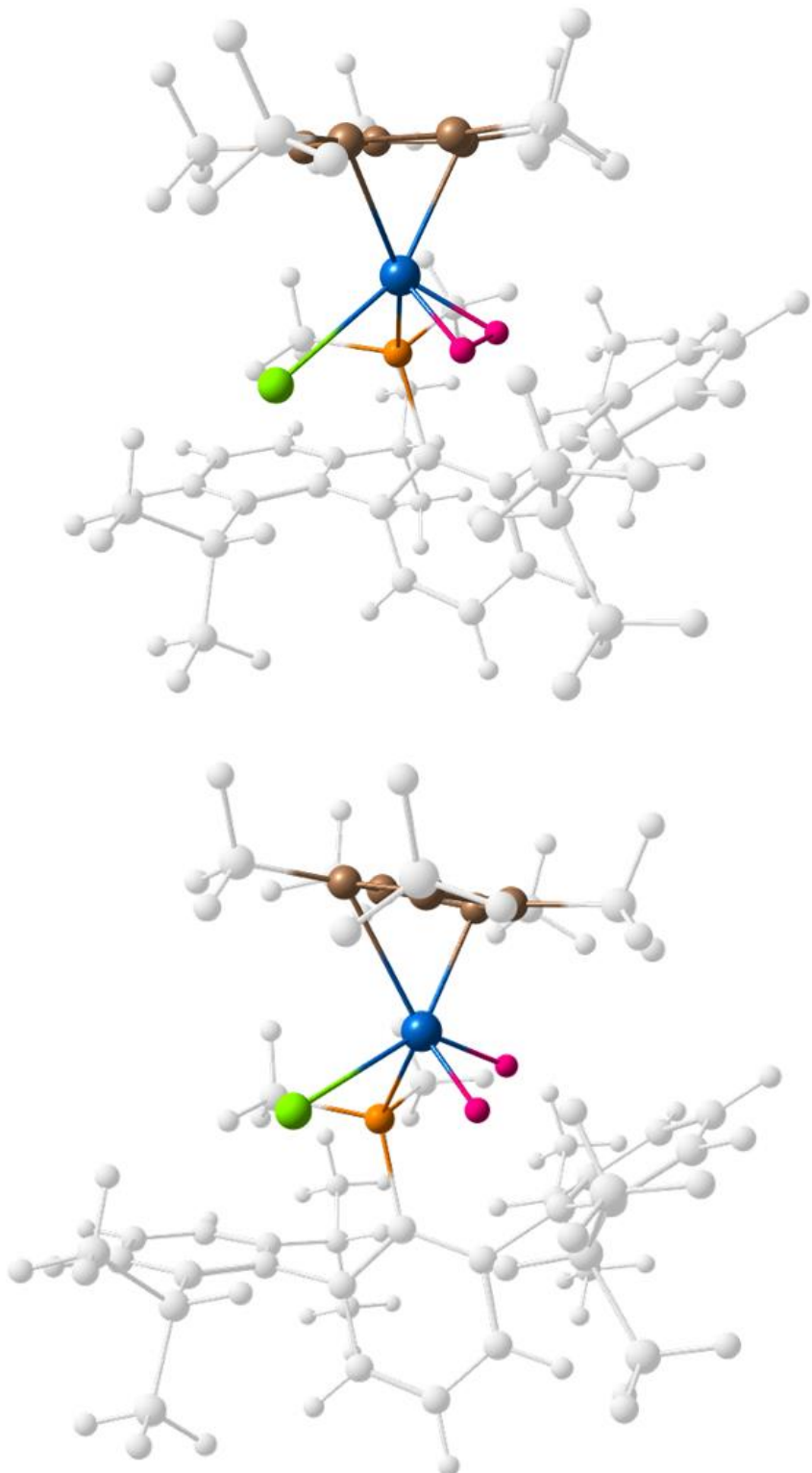


Figure S11. Calculated molecular geometries of $\mathbf{1} \cdot (\sigma\text{-H}_2)^+$ (top) and $\mathbf{1} \cdot (\text{H}_2)_2^+$.

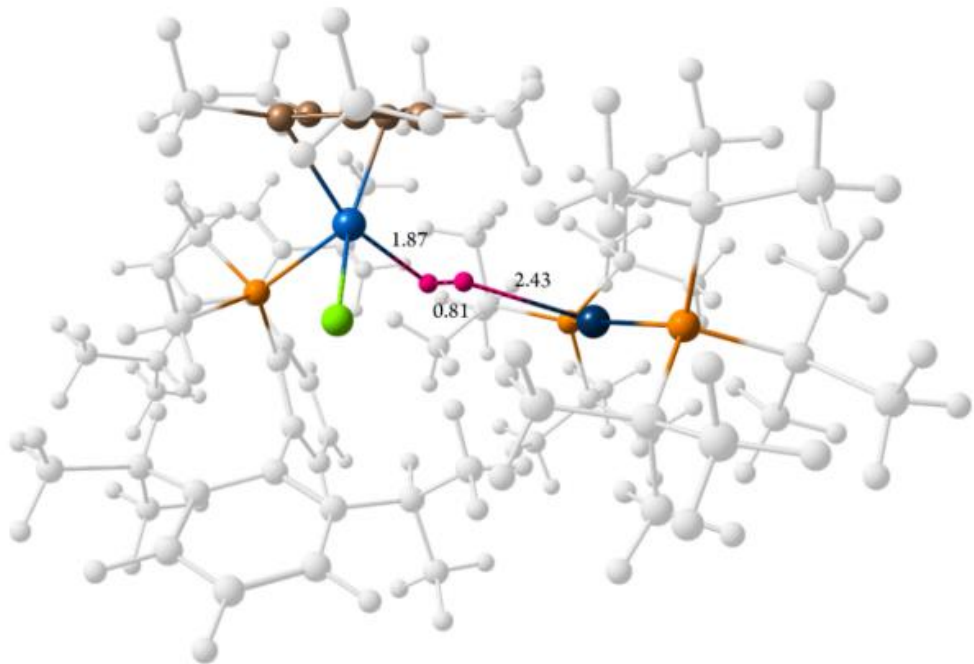


Figure S12. Molecular geometry of the transition state for the FLP-type H₂ splitting.

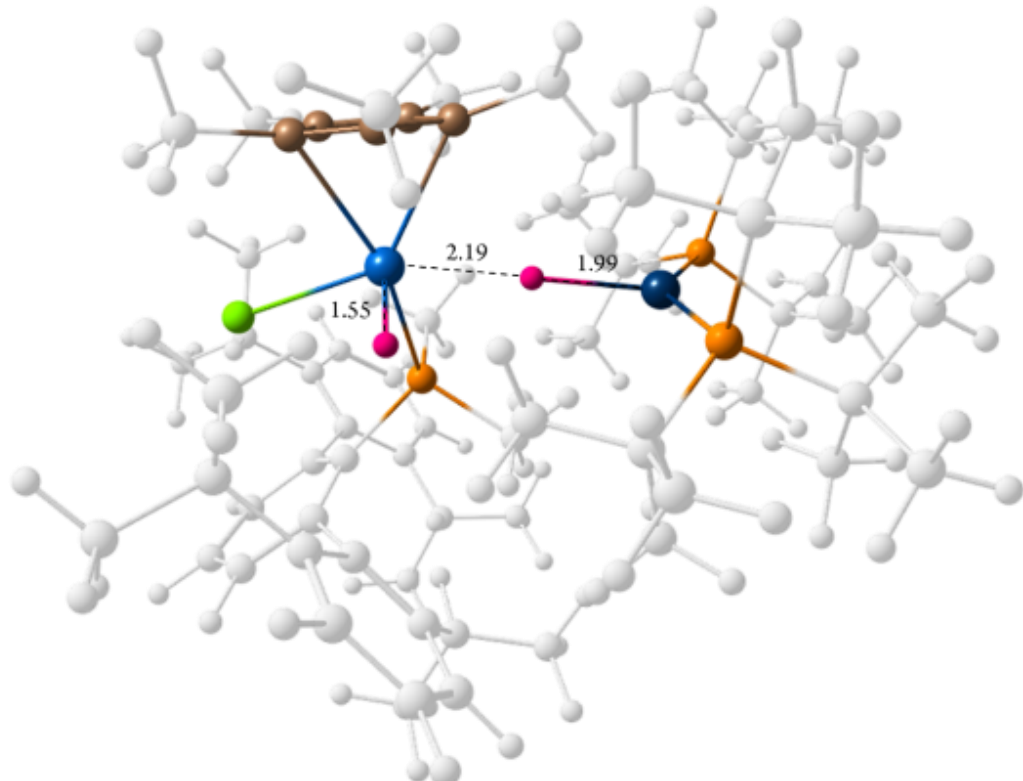


Figure S13. Molecular geometry of the transition state for the Pt-mediated deprotonation of 1·(H)2⁺

5. References

- [1] G. M. Sheldrick, *Acta Crystallogr. Section C*, **2015**, *71*, 3–8.
- [2] O. V. Dolomanov, L. J. Bourhis, R. J. Gildea, J. A. K. Howard, H. Puschmann, *J. Appl. Crystallogr.*, **2009**, *42*, 339–341.
- [3] L. J. Bourhis, O. v Dolomanov, R. J. Gildea, J. A. K. Howard, H. Puschmann, *Acta Crystallogr. Section A*, **2015**, *71*, 59–75.
- [4] G. M. Sheldrick, *Acta Crystallogr. Section A*, **2008**, *64*, 112–122.
- [5] M. J. Frisch, G. W. Trucks, H. B. Schlegel, G. E. Scuseria, M. A. Robbs, . J. R. Cheeseman, G. Scalmani, V. Barone, B. Mennucci, G. A. Petersson, H. Nakatsuji, M. Caricato, X. Li, H. P. Hratchian, A. F. Izmaylov, J. Bloino, G. Zheng, J. L. Sonnenberg, M. Hada, M. Ehara, K. Toyota, R. Fukuda, J. Hasegawa, M. Ishida, T. Nakajima, Y. Honda, O. Kitao, H. Nakai, T. Vreven, J. A. J. Montgomery, J. E. Peralta, F. Ogliaro, M. Bearpark, J. J. Heyd, E. Brothers, K. N. Kudin, V. N. Staroverov, R. Kobayashi, J. Normand, K. Raghavachari, A. Rendell, J. C. Burant, S. S. Iyengar, J. Tomasi, M. Cossi, N. Rega, J. M. Millam, M. Klene, J. E. Knox, J. B. Cross, V. Bakken, C. Adamo, J. Jaramillo, R. Gomperts, R. E. Stratmann, O. Yazyev, A. J. Austin, R. Cammi, C. Pomelli, J. W. Ochterski, R. L. Martin, K. Morokuma, V. G. Zakrzewski, G. A. Voth, P. Salvador, J. J. Dannenberg, S. Dapprich, A. D. Daniels, O. Farkas, J. B. Foresman, J. V. Ortiz, J. Cioslowski, D. Fox. Gaussian 09. Gaussian, Inc.: Wallingford CT **2009**.
- [6] J. P. Perdew, K. Burke, M. Ernzerhof, *Phys. Rev. Lett.* **1996**, *77*, 3865–3869.
- [7] a) R. Ditchfield, W. J. Hehre, J. A. Pople. *J. Chem. Phys.* **1971**, *54*, 724–728; b) W. J. Hehre, R. Ditchfield, J. A. Pople. *J. Chem. Phys.* **1972**, *56*, 2257–2261; c) P. C. Hariharan, J. A. Pople. *Theor. Chim. Acta* **1973**, *28*, 213–222; d) M. M. Franci, W. J. Pietro, W. J. Hehre, J. S. Binkley, M. S. Gordon, D. J. DeFrees, J. A. Pople. *J. Chem. Phys.* **1982**, *77*, 3654–3665.
- [8] D. Andrae, U. Häußermann, M. Dolg, H. Stoll, H. Preuß. *Theor. Chim. Acta* **1990**, *77*, 123–141.
- [9] A. V. Marenich, C. J. Cramer, D. G. Truhlar. *J. Phys. Chem. B* **2009**, *113*, 6378–6396.
- [10] S. Grimme, J. Antony, S. Ehrlich, H. Krieg, *J. Chem. Phys.*, **2010**, *132*, 154104.
- [11] (a) J. Kua, H. E. Krizner, D. O. De Haan, *J. Phys. Chem. A*, **2011**, *115*, 1667; b) L.-L. Han, S.-J. Li, D.-C. Fang, *Phys. Chem.*, **2016**, *18*, 6182.
- [12] (a) P. Ríos, A. Rodríguez, J. López-Serrano, *ACS Catal.* **2016**, *6*, 5715; (b) D. V. Deubel, *J. Am. Chem. Soc.* **2008**, *130*, 665.